

LETTER TO THE EDITOR

Interstellar CH absorption in the diffuse interstellar medium along the sight-lines to G10.6–0.4 (W31C), W49N, and W51^{★,★★}

M. Gerin¹, M. De Luca¹, J. R. Goicoechea², E. Herbst³, E. Falgarone¹, B. Godard^{1,4}, T. A. Bell⁵, A. Coutens^{6,7}, M. Kaźmierczak⁸, P. Sonnentrucker⁹, J. H. Black¹⁰, D. A. Neufeld⁹, T. G. Phillips⁵, J. Pearson¹¹, P. B. Rimmer³, G. Hassel³, D. C. Lis⁵, C. Vastel^{6,7}, F. Boulanger⁴, J. Cernicharo², E. Dartois⁴, P. Encrenaz¹, T. Giesen¹², P. F. Goldsmith¹¹, H. Gupta¹¹, C. Gry¹³, P. Hennebelle¹, P. Hily-Blant¹⁴, C. Joblin^{6,7}, R. Kłos¹⁵, J. Krełowski⁸, J. Martín-Pintado², R. Monje⁵, B. Mookerjee¹⁶, M. Perault¹, C. Persson¹⁰, R. Plume¹⁷, M. Salez¹, M. Schmidt¹⁸, J. Stutzki¹², D. Teyssier¹⁹, S. Yu¹¹, A. Contursi²⁰, K. Menten²¹, T. R. Geballe²², S. Schlemmer¹², P. Morris²³, W. A. Hatch¹¹, M. Imram¹¹, J. S. Ward¹¹, E. Caux^{6,7}, R. Güsten²¹, T. Klein²¹, P. Roelfsema²⁴, P. Dieleman²⁴, R. Schieder¹², N. Honingh¹², and J. Zmuidzinas⁵

(Affiliations are available on page 5 of the online edition)

Received 31 May 2010 / Accepted 9 July 2010

ABSTRACT

We report the detection of the ground state $N, J = 1, 3/2 \rightarrow 1, 1/2$ doublet of the methylidyne radical CH at ~ 532 GHz and ~ 536 GHz with the *Herschel*/HIFI instrument along the sight-line to the massive star-forming regions G10.6–0.4 (W31C), W49N, and W51. While the molecular cores associated with these massive star-forming regions show *emission* lines, clouds in the diffuse interstellar medium are detected in *absorption* against the strong submillimeter background. The combination of hyperfine structure with emission and absorption results in complex profiles, with overlap of the different hyperfine components. The opacities of most of the CH absorption features are linearly correlated with those of CCH, CN, and HCO⁺ in the same velocity intervals. In specific narrow velocity intervals, the opacities of CN and HCO⁺ deviate from the mean trends, giving rise to more opaque absorption features. We propose that CCH can be used as another tracer of the molecular gas in the absence of better tracers, with $[CCH]/[H_2] \sim 3.2 \pm 1.1 \times 10^{-8}$. The observed $[CN]/[CH]$, $[CCH]/[CH]$ abundance ratios suggest that the bulk of the diffuse matter along the lines of sight has gas densities $n_H = n(H) + 2n(H_2)$ ranging between 100 and 1000 cm⁻³.

Key words. ISM: clouds – ISM: molecules – submillimeter: ISM – ISM: individual objects: G10.6-0.4 – ISM: individual objects: W49N – ISM: individual objects: W51

1. Introduction

The methylidyne radical was detected in the interstellar medium as early as 1937 (Swings & Rosenfeld 1937). Since then, it has remained one of the most studied interstellar molecules through its electronic transitions at 430 nm. CH is now established as a powerful tracer of molecular hydrogen, with a tight correlation over nearly two decades of column density $[CH]/[H_2] = 3.5 \times 10^{-8}$ (Sheffer et al. 2008). While optical spectroscopy can reach excellent spectral resolution, it is limited to relatively bright objects and cannot sample the full variety of interstellar environments. Radio observations are thus an interesting complement to optical spectroscopy. Qin et al. (2010) discuss the CH spectroscopy, and the energy level diagram of CH is shown in Naylor et al. (2010). The lambda doubling transitions at 3 GHz are relatively easily detected at cm wavelengths, but their quantitative interpretation is difficult because they show anomalous

excitation (Liszt & Lucas 2002, and references therein). The CH rotational lines lie at submillimeter and far-infrared wavelengths, with a characteristic doublet pattern. While the first observations were obtained with the Kuiper Airborne Observatory (KAO) by Stacey et al. (1987) towards the massive region Sgr B2 in the Galactic center, these transitions attracted little attention until the 149 μ m CH doublet was identified in many ISO-LWS spectra (Goicoechea et al. 2004; Polehampton et al. 2005).

In the framework of gas-phase ion-molecule chemistry, the formation of CH is initiated by the slow radiative association between ionised carbon C⁺ and molecular hydrogen H₂, leading to CH₂⁺, because the direct reaction to form CH⁺ faces an energy barrier of ~ 4640 K (Black & Dalgarno 1973; Godard et al. 2009).

In low-density gas illuminated by ultraviolet radiation, the reaction of C⁺ with vibrationally excited H₂ is not efficient enough to bypass the radiative association reaction (Agundez et al. 2010). Once formed, CH₂⁺ rapidly reacts with H₂ to form CH₃⁺, a key precursor of many interstellar hydrocarbons. CH results from the dissociative recombination of both CH₂⁺ and CH₃⁺. It is expected theoretically, and verified by the observations, that the CH column density will scale with the H₂ column density

[★] *Herschel* is an ESA space observatory with science instruments provided by European-led Principal Investigator consortia and with important participation from NASA.

^{★★} Appendices A and B (pages 6, 7) are only available in electronic form at <http://www.aanda.org>

in regions where the chemistry is dominated by the ultraviolet radiation (Cardelli et al. 1991; Sheffer et al. 2008).

The chemistry of the diffuse interstellar medium cannot be entirely captured by the simple framework described above, as reactions on surfaces and transient processes may play important roles, too. For example, the energy release mediated by magnetic fields in the dissipation regions of strong interstellar turbulence may drive a “warm chemistry” where reactions that would otherwise be inhibited at low temperature become important (Godard et al. 2009). The methylidyne ion, CH^+ , is predicted to arise in such turbulent dissipation regions. There is already observational evidence that some fraction of the CH forms from CH^+ (Pan et al. 2005), in addition to the quiescent, photon-dominated source discussed above. We present here a comparison of CH with other carbon species present in the diffuse interstellar medium, HCO^+ , CN, and CCH towards the targets, W31C, W51, and W49N (Table 2).

2. Observations

The observations were performed with the *Herschel*/HIFI instrument (de Graauw et al. 2010) in 2010 March and April. The data were taken in double beam switching (DBS) mode with a throw of 3 arc-min. To remove the ambiguity on the line frequency in observations performed with double side band mixers, each line was observed with three settings of the local oscillator (LO). We used the two HIFI spectrometers: the wide band spectrometer (WBS) that provides a total bandwidth of 4 GHz, with 1.1 MHz spectral resolution (0.56 km s^{-1} at 532 GHz), and the high resolution spectrometer (HRS) with 0.12 MHz spectral resolution. The on-source integration times have been set to reach a S/N ratio on the continuum of at least 50 for a velocity resolution of 1 km s^{-1} . This translates into observing times of 23, 7.5 and 11 min for G10.6–0.4, W49N and W51, respectively, for each CH line.

The spectra were calibrated with a hot and cold blackbody (Roelfsema et al. 2010). because we are interested in the absorption, we have not corrected the data for the main beam efficiency. The data were first processed using HIPE (Ott et al. 2010), and subsequently exported to CLASS (Hily-Blant et al. 2005; Pety 2005). For each source, the data obtained with the three LO settings were in excellent agreement (better than 10%) and could be co-added. The spectra obtained from the H and V polarization mixers agreed well. The continuum levels agree well for both polarizations, but do not generally coincide. At 532 GHz, we obtained a double side band continuum T_c of $0.94 \pm 0.03 \text{ K}$, $1.5 \pm 0.5 \text{ K}$ and $1.8 \pm 0.1 \text{ K}$ for G10.6–0.4, W49N, and W51. We produced normalized spectra as $I = 2(T - T_c/2)/T_c$, where T stands for the antenna temperature, and we assume that the relative gains of the lower and upper side bands are equal. The H and V normalized spectra were finally co-added to produce the spectra shown in Figs. 1–3.

For both CH triplets, the line profiles are complex because the emission or absorption of each of the three hyperfine components overlaps partly with the signal from the other components. High spectral resolution data are therefore a prerequisite to properly derive the CH column densities in complex sources. To properly separate the foreground absorption and extract the velocity structure of the absorbing gas, we have taken advantage of the known frequency offsets of the hyperfine components to “deconvolve” the spectra from the hyperfine structure. We have written the normalized spectra as $I = e^{-\sum_{i=1}^3 \alpha_i \tau_i}$, hence $-\ln(I) = \sum_{i=1}^3 \alpha_i \tau_i$, where $\tau_i = \alpha_i \tau_m$ stands for the opacity of the hyperfine component $\#i$, and α_i is the intensity of this component relative to the main one. This formula uses the assumption

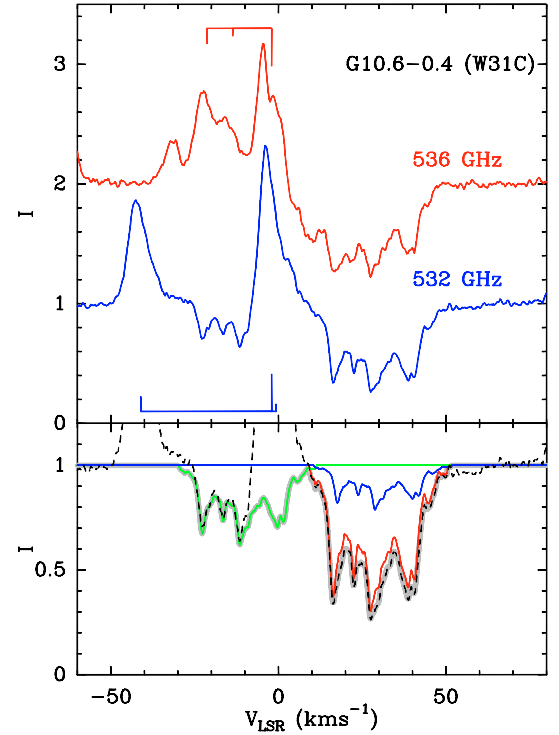


Fig. 1. *Top:* normalized spectra of the CH transitions at 532 GHz and 536 GHz towards G10.6–0.4. The 536 GHz spectrum has been shifted by 1 for clarity. *Bottom:* decomposition of the 532 GHz line into three hyperfine components, the red line shows the main component, the blue and green lines the satellites, and the grey curve the sum of the three components. The data are shown with a black dashed line.

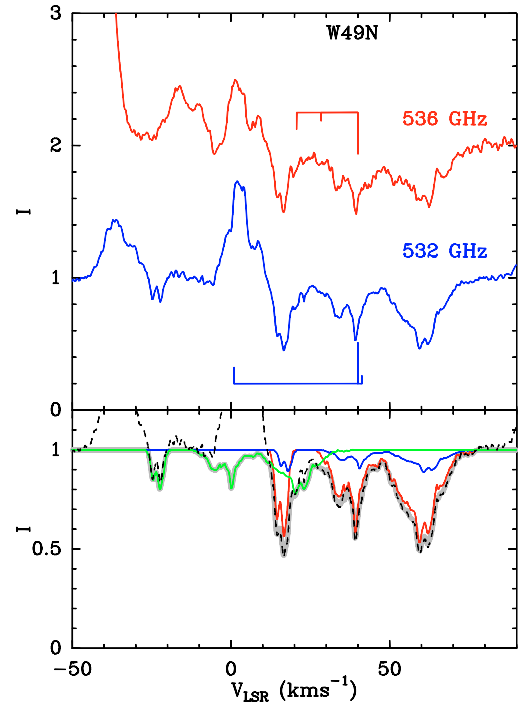


Fig. 2. Same as Fig. 1 for W49N.

that the ratios of the opacities of the CH hyperfine components follow the relative intensities, i.e., there is no anomalous excitation of the hyperfine levels. In regions of the spectrum where the main hyperfine component is blended with satellite lines from another velocity component, its opacity can be deduced from

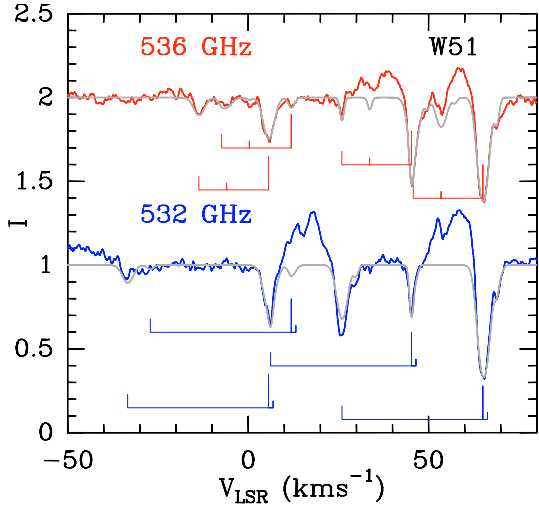


Fig. 3. Normalized spectra of the CH transitions at 532 GHz and 536 GHz towards W51. The 536 GHz spectrum has been shifted for clarity. The grey lines show the model, the positions of the CH triplets for the four velocity components are indicated below each transition.

the opacity of the satellite lines in “clean” spectral regions. The deconvolution method was performed on either the 532 GHz or the 536 GHz triplets depending on the source. We checked that the resulting velocity structure agrees with the observations of the other triplet. The bottom panels in Figs. 1 and 2 show the absorption profiles for each hyperfine component overlaid on the data. For W51 (Fig. 3), the overlap of the hyperfine components is not as severe as for the other sources, and we fitted the 532 GHz absorption profile with four Gaussian velocity components. We used the position and width as derived from the fit of the HF and HCO⁺ spectra (Sonnentrucker et al. 2010; Godard et al. 2010).

3. Results

We used the profile of the main hyperfine component of CH to derive the properties of the absorbing material. At first sight, the CH profile is similar to those of ground state transitions of simple molecules like HF and H₂O (Neufeld et al. 2010a; Sonnentrucker et al. 2010; Lis et al. 2010), HCO⁺, CN, CCH, and c-C₃H₂ (Godard et al. 2010; Gerin et al. 2010b), OH⁺ and CH⁺ (Neufeld et al. 2010b; Gerin et al. 2010a; Falgarone et al. 2010). To be more quantitative, we show in Fig. 4 comparisons of the opacities of the main spin-rotation-hyperfine component of CH($N = 1 \leftarrow 1$), CCH($N = 1 \leftarrow 0$, 87316.898 MHz), CN($N = 1 \leftarrow 0$ 113191.2787 MHz), and of the $J = 1-0$ line of HCO⁺ in selected velocity intervals. Each point corresponds to one velocity channel in the spectra. We have arbitrarily set the maximum value of opacity of the HCO⁺ data to 3.5 because the observations are not sensitive to opacities larger than ~ 3 . For all lines of sight the plots present the same structure: a general linear trend and strong deviations in narrow velocity intervals where the CN and HCO⁺, and to a lesser extent CCH, opacities, get larger than the average for a given CH opacity. Since CH is expected to be linearly correlated with H₂, an increase in the total column density cannot explain these sharp features. As discussed by Sheffer et al. (2008), it is more likely that the sharp features are associated with regions of higher-than-average density along the lines of sight. It is known that the CN abundance is sensitive to the gas density in diffuse clouds

Table 1. CH spectroscopic parameters for the $N = 1 \leftarrow 1$ transitions.

Frequency MHz	Transition $J', F' \leftarrow J'', F''$	A_{ul} 10^{-4} s^{-1}	E_u/k K	$\int \tau dV/N^a$ $10^{-13} \text{ km s}^{-1} \text{ cm}^2$	V_{off} km s^{-1}
532721.68	$3/2, 1^+ \leftarrow 1/2, 1^-$	2.07	25.7	0.055	1.3
532723.93	$3/2, 2^+ \leftarrow 1/2, 1^-$	6.21	25.7	0.275	0.0
532793.31	$3/2, 1^+ \leftarrow 1/2, 0^-$	4.14	25.7	0.110	-39.0
536761.15	$3/2, 2^- \leftarrow 1/2, 1^+$	6.38	25.8	0.276	0.0
536781.95	$3/2, 1^- \leftarrow 1/2, 1^+$	2.13	25.8	0.055	-11.6
536795.68	$3/2, 1^- \leftarrow 1/2, 0^+$	4.25	25.8	0.111	-19.3

Notes. ^(a) Opacity integrated over the line profile per total CH column density, under the assumption that $T_{\text{ex}} \ll E_u/k$.

Table 2. Source parameters.

Name	RA J2000	DEC J2000	V_{LSR} km s^{-1}	N_{H}^a 10^{22} cm^{-2}	$N(\text{H})$ 10^{22} cm^{-2}
W31C ^b	18:10:28.7	-19:55:50.0	-2	2.7	1.2
W49N	19:10:13.2	09:06:12	11	4.1	1.4
W51 ^c	19:23:43.9	14:30:30.5	57	2.5	0.8

Notes. ^(a) Total hydrogen: $N_{\text{H}} = 2N(\text{H}_2) + N(\text{H})$, see text. ^(b) Also known as G10.6-0.64. ^(c) W51-E4.

(Cardelli et al. 1991; Federman et al. 1994). The *Herschel* data nicely confirm the results of optical spectroscopy.

The linear trends in optical depth show that the ratios of molecular column densities stay in a narrow range for the three sources we have sampled. At the densities typical of diffuse gas, $n(\text{H}_2) \lesssim 10^3 \text{ cm}^{-3}$, the rotational excitation of CH is controlled mainly by radiative processes so that the excitation temperatures of the 532 and 536 GHz transitions are expected to be $T_{\text{ex}} \approx 3.1 \text{ K}$ in the average Galactic background radiation. For these unsaturated submillimeter transitions $T_{\text{ex}} \ll hv/k$ and almost all CH molecules are in the lowest rotational state; therefore, we expect a simple relationship between the integrated absorption $\int \tau dV$ and the total column density of CH, $N(\text{CH})$ (see Table 1). Low-lying excited states are populated in the heavier molecules CN, CCH, and HCO⁺, but the rotational excitation temperatures are expected to remain in the range 2.73 to 3.1 K, low enough that column densities are simply related to integrated absorption when the lines are unsaturated. These linear relations between opacity and column density have been tested by means of non-LTE excitation calculations that include collisions by neutrals and electrons as well as radiative excitation in the average Galactic background continuum (cf. van der Tak et al. 2007). We find ratios of column densities $N(\text{CCH})/N(\text{CH}) = 0.6-1.2$ with values of up to 1.8, and $N(\text{CN})/N(\text{CH}) = 0.5-1$ with values of up to 3. The HCO⁺ spectra are more saturated, but follow the same trends. We find $N(\text{HCO}^+)/N(\text{CH}) = 0.04-0.08$ with values of up to at least 0.2. The [CN]/[CH] ratio lies at the upper end of the values derived from optical spectroscopy (Sheffer et al. 2008; Weselak et al. 2008).

As further described in the appendix, we have used the Meudon-PDR code (Le Petit et al. 2006; Goicoechea & Le Bourlot 2007; Gonzalez Garcia et al. 2008) to study how these abundance ratios depend on the gas density. The [CN]/[CH] and [CCH]/[CH] abundance ratios are sensitive to the gas density as suggested by Cardelli et al. (1991). For the bulk of the diffuse matter producing the absorption features, the observations are consistent with gas densities between 100 and 1000 cm^{-3} .

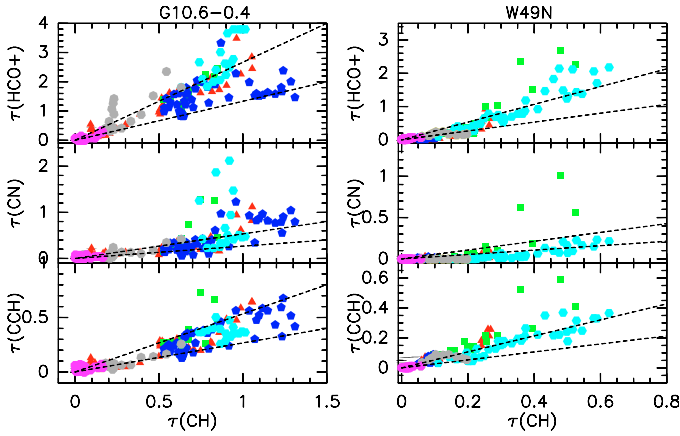


Fig. 4. Comparison of the opacity of the main CH hyperfine component with those of the CCH, CN, and HCO⁺ ground-state millimeter-wave transitions. Each point corresponds to a 0.5 km s⁻¹ velocity channel. Dashed lines indicate the minimum and maximum ratios in the linear trend. For G10.6-0.4, the velocity range 12–22 km s⁻¹ is shown in red, 22–25 km s⁻¹ in green, 25–38 km s⁻¹ in blue, 38–43 km s⁻¹ in cyan, 43–48 km s⁻¹ in grey and 48–60 km s⁻¹ in purple. For W49N, the velocity range 30–36 km s⁻¹ is shown in red, 36–43 km s⁻¹ in green, 43–50 km s⁻¹ in blue, 50–67 km s⁻¹ in cyan, 67–71 km s⁻¹ in grey and 71–78 km s⁻¹ in purple.

The CH column densities for selected velocity intervals are reported in Table A.1, together with the H₂ column densities, assuming the mean CH abundance [CH]/[H₂] = 3.5 × 10⁻⁸ (Sheffer et al. 2008). The deduced total H₂ column densities are N(H₂) = 1.6 × 10²² cm⁻², 1.1 × 10²² cm⁻² and 0.16 × 10²² cm⁻² for G10.6–0.4, W49N, and W51 respectively. The total hydrogen column can be estimated independently from the K-band extinction (Marshall et al. 2006), and the atomic hydrogen column from the HI 21 cm line data (Godard et al. 2010; Sonnentrucker et al. 2010), as listed in Table 2. This second method yields N(H₂) = 0.75 × 10²² cm⁻², 1.3 × 10²² cm⁻² and 0.85 × 10²² cm⁻². Given the scatter in the [CH]/[H₂] relation (0.2 dex corresponding to a factor of 1.6) and the uncertainties in total extinction, the two methods agree well for G10.6–0.4 and W49N. The total H column may be overestimated towards W51. A likely explanation is that the quoted figure includes extinction directly associated with the W51 molecular complex itself, which could be related to the 65 km s⁻¹ velocity feature (Koo 1997). Our analysis of three sight-lines suggests that the abundance of CH relative to H₂ in the Galactic disk is similar to that in the Solar neighbourhood.

CCH appears to be better correlated with CH than either CN or HCO⁺. Therefore we suggest that CCH can be used as another tracer of molecular hydrogen, which is easily observable from the ground and complements CH and HF. Assuming that the mean CH abundance relative to H₂ derived by Sheffer et al. (2008) holds in the Galactic plane, we derive [CCH]/[H₂] = (3.2 ± 1.1) × 10⁻⁸, which excellently agrees with the abundance estimated by Lucas & Liszt (2000).

4. Conclusion

Unlike lines of other hydrides, CH submillimeter absorption lines in the diffuse matter are not saturated, a feature already identified in the ISO-LWS spectra of the CH ground state transitions at 149 μm. This makes CH a powerful tracer of the diffuse molecular gas along Galactic lines of sight, which complements HF (Neufeld et al. 2010a; Sonnentrucker et al. 2010). We

show that the column densities of simple molecules (CN, CCH, HCO⁺) are well correlated with those of CH except in some narrow velocity ranges where significantly higher column densities than average are derived, especially for CN and HCO⁺. This behaviour may trace the densest regions along the line of sight. The bulk of the matter lies at n_H = 100–1000 cm⁻³. We propose that CCH can be used as a complementary tracer of H₂, with [CCH]/[H₂] = (3.2 ± 1.1) × 10⁻⁸.

Acknowledgements. HIFI has been designed and built by a consortium of institutes and university departments from across Europe, Canada, and the United States under the leadership of SRON, the Netherlands Institute for Space Research, Groningen, The Netherlands, and with major contributions from Germany, France and the US. Consortium members are: Canada: CSA, U. Waterloo; France: CESR, LAB, LERMA, IRAM; Germany: KOSMA, MPIfR, MPS; Ireland: NUI Maynooth; Italy: ASI, IFSI-INAF, Osservatorio Astrofisico di Arcetri-INAF; Netherlands: SRON, TUD; Poland: CAMK, CBK; Spain: Observatorio Astronómico Nacional (IGN), Centro de Astrobiología; Sweden: Chalmers University of Technology – MC2, RSS & GARD, Onsala Space Observatory, Swedish National Space Board, Stockholm University – Stockholm Observatory; Switzerland: ETH Zurich, FHNW; USA: CalTech, JPL, NHSC. M.G., E.F., M.D.L. acknowledge the support from the Centre National de Recherche Spatiale (CNES), and from ANR through the SCHISM project (ANR-09-BLAN-231). JRG was supported by a Ramon y Cajal contract and by the MICINN/AYA2009-07304 and CSD2009-00038 grants.

References

- Agúndez, M., Goicoechea, J. R., Cernicharo, J., et al. 2010, *ApJ*, 713, 662
 Black, J. H., & Dalgarno, A. 1973, *ApJ*, 15, L79
 Cardelli, J., Federman, S. R., & Smith, V. V. 1991, *ApJ*, 381, L17
 de Graauw, Th., Helmich, F. P., Phillips, T. G., et al. 2010, *A&A*, 518, L6
 Falgarone, E., Godard, B., Cernicharo, J., et al. 2010, *A&A*, 521, L15
 Federman, S. R. 1982, *ApJ*, 257, 125
 Federman, S. R., Strom, C. J., Lambert, D. L., et al. 1994, *ApJ*, 424, 772
 Gerin, M., Kaźmierczak, M., Jastrzebska, M., et al. 2010a, *A&A*, submitted
 Gerin, M., de Luca, M., Black, J., et al. 2010b, *A&A*, 518, L110
 Godard, B., Falgarone, E., & Pineau des Forêts, G. 2009, *A&A*, 495, 847
 Godard, B., Falgarone, E., Gerin, M., Hily-Blant, P., & De Luca, M. 2010, *A&A*, 520, A20
 Goicoechea, J. R., Rodríguez-Fernández, N. J., & Cernicharo, J. 2004, *ApJ*, 600, 214
 Goicoechea, J. R., & Le Bourlot, J. 2007, *A&A*, 467, 1
 Gonzalez Garcia, M., Le Bourlot, J., Le Petit, F., & Roueff, E. 2008, *A&A*, 485, 127
 Hily-Blant, P. 2005, IRAM internal report
 Koo, B.-C. 1997, *ApJS*, 108, 489
 Le Petit, F., Nehmé, C., Le Bourlot, J., & Roueff, E. 2006, *ApJS*, 164, 506
 Lis, D. C., Phillips, T. G., Neufeld, D. A., et al. 2010, *A&A*, 521, L26
 Liszt, H., & Lucas, R. 2002, *A&A*, 391, 693
 Lucas, R., & Liszt, H. S. 2000, *A&A*, 358, 1069
 Marshall, D. J., Robin, A. C., Reylé, C., et al. 2006, *A&A*, 453, 635
 Naylor, D. A., Dartois, E., Habart, E., et al. 2010, *A&A*, 518, L117
 Neufeld, D., Sonnentrucker, P., Phillips, T. G., et al. 2010, *A&A*, 518, L108
 Neufeld, D., Goicoechea, J. R., Sonnentrucker, P., et al. 2010, *A&A*, 521, L10
 Ott, S. 2010, in *Astronomical Data Analysis Software and Systems XIX*, ed. Y. Mizuno, K. I. Morita, & M. Ohishi, ASP Conf. Ser.
 Pan, K., Federman, S. R., Sheffer, Y., & Andersson, B.-G. 2005, *ApJ*, 633, 986
 Pety, J. 2005, SF2A conference, ed. F. Casoli, T. Contini, J. M. Hameury, & L. Pagani, EDP-Sciences Conf. Ser.
 Pilbratt, G. L., Riedinger, J. R., Passvogel, T., et al. 2010, *A&A*, 518, L1
 Polehampton, E., Menten, K. M., Brünken, S., Winnewisser, G., & Baluteau, J.-P. 2005, *A&A*, 431, 203
 Qin, S.-L., Schilke, P., Comito, C., et al. 2010, *A&A*, 521, L14
 Roelfsema, P. R., Helmich, F. P., Teyssier, D., et al. 2010, *A&A*, submitted
 Sheffer, Y., Rogers, M., & Federman, S. R. 2008, *ApJ*, 687, 1075
 Sonnentrucker, P., Neufeld, D. A., Phillips, T. G., et al. 2010, *A&A*, 521, L12
 Stacey, G. J., Lugten, J. B., & Genzel, R. 1987, *ApJ*, 313, 859
 Swings, P., & Rosenfeld, L. 1937, *ApJ*, 86, 483
 van der Tak, F. F. S., Black, J. H., Schöier, F. L., Jansen, D. J., & van Dishoeck, E. F. 2007, *A&A*, 468, 627
 Weselak, T., Galazutdinov, G. A., Beletsky, Y., & Krelowski, J. 2008, *A&A*, 484, 381

-
- ¹ LERMA, CNRS, Observatoire de Paris and ENS, France
e-mail: maryvonne.gerin@ens.fr
- ² Centro de Astrobiología, CSIC-INTA, Madrid, Spain
- ³ Depts. of Physics, Astronomy & Chemistry, Ohio State Univ., USA
- ⁴ Institut d'Astrophysique Spatiale (IAS), Orsay, France
- ⁵ California Institute of Technology, Pasadena, CA 91125, USA
- ⁶ Université de Toulouse; UPS; CESR; 9 avenue du colonel Roche, 31028 Toulouse Cedex 4, France
- ⁷ CNRS; UMR5187; 31028 Toulouse, France
- ⁸ Nicolaus Copernicus University, Torún, Poland
- ⁹ The Johns Hopkins University, Baltimore, MD 21218, USA
- ¹⁰ Chalmers University of Technology, Onsala Space Observatory, 43992 Onsala, Sweden
- ¹¹ JPL, California Institute of Technology, Pasadena, USA

- ¹² I. Physikalisches Institut, University of Cologne, Germany
- ¹³ Laboratoire d'Astrophysique de Marseille (LAM), France
- ¹⁴ Laboratoire d'Astrophysique de Grenoble, France
- ¹⁵ Institute of Physical Chemistry, Polish Academy of Sciences, Warsaw, Poland
- ¹⁶ Tata Institute of Fundamental Research, Mumbai, India
- ¹⁷ Dept. of Physics & Astronomy, University of Calgary, Canada
- ¹⁸ Nicolaus Copernicus Astronomical Center, Poland
- ¹⁹ European Space Astronomy Centre, ESA, Madrid, Spain
- ²⁰ MPI für Extraterrestrische Physik, Garching, Germany
- ²¹ MPI für Radioastronomie, Bonn, Germany
- ²² Gemini telescope, Hilo, Hawaii, USA
- ²³ Infrared Processing and Analysis Center, California Institute of Technology, MS 100-22, Pasadena, CA 91125, USA
- ²⁴ SRON Netherlands Institute for Space Research, Netherlands

Appendix A: CH column densities

Table A.1. CH column densities.

Name	V_{\min} km s^{-1}	V_{\max} km s^{-1}	$N(\text{CH})$ 10^{13} cm^{-2}	$N(\text{H}_2)^a$ 10^{21} cm^{-2}
G10.6–0.64 (W31C)	10	20	14 ± 1	3.9
	20	25	9.8 ± 1	2.7
	25	35	26 ± 1	7.3
	25	42	17 ± 1	4.8
	42	47	3.3 ± 1	0.9
W49N	30	50	13 ± 1	3.7
	50	78	24 ± 1	6.6
	67	71	1.5 ± 0.2	0.4
W51	3	10	3.7 ± 0.2	1.0
	10	15	0.5 ± 0.15	0.14
	42	47	1.8 ± 0.15	0.5

Notes. ^(a) Based on $[\text{CH}]/[\text{H}_2] = 3.5 \times 10^{-8}$ (Sheffer et al. 2008).

Appendix B: PDR models

Figure B.1 presents models produced using the Meudon PDR code, a steady-state, depth-dependent model of a plane-parallel cloud (Le Petit et al. 2006; Goicoechea & Le Bourlot 2007; Gonzalez Garcia et al. 2008). Our chemical network is based on a modified version of the Ohio State University (OSU) gas-phase network updated for photochemical studies. We have computed the thermal and chemical structure of diffuse clouds with $A_V < 5$, $n_{\text{H}} = 100\text{--}5000 \text{ cm}^{-3}$, cosmic ray ionization rates ζ_{H} of 10^{-17} s^{-1} , 10^{-16} s^{-1} , and 10^{-15} s^{-1} , and illuminated only at one side by a UV field, χ , between 1 and 10 times the mean interstellar radiation field (in Draine units). The $[\text{CN}]/[\text{CH}]$, $[\text{HCO}^+]/[\text{CH}]$ and $[\text{C}_2\text{H}]/[\text{CH}]$ ratios are sensitive to the gas density as suggested by Cardelli et al. (1991). For the bulk of the diffuse matter producing absorption features, the observations are consistent with gas densities between 100 and 1000 cm^{-3} . Figure B.1 also shows the predicted scaling between CH and H_2 column densities in the parameter space appropriate for diffuse clouds. An approximately similar trend is predicted for C_2H when $A_V > 0.01$.

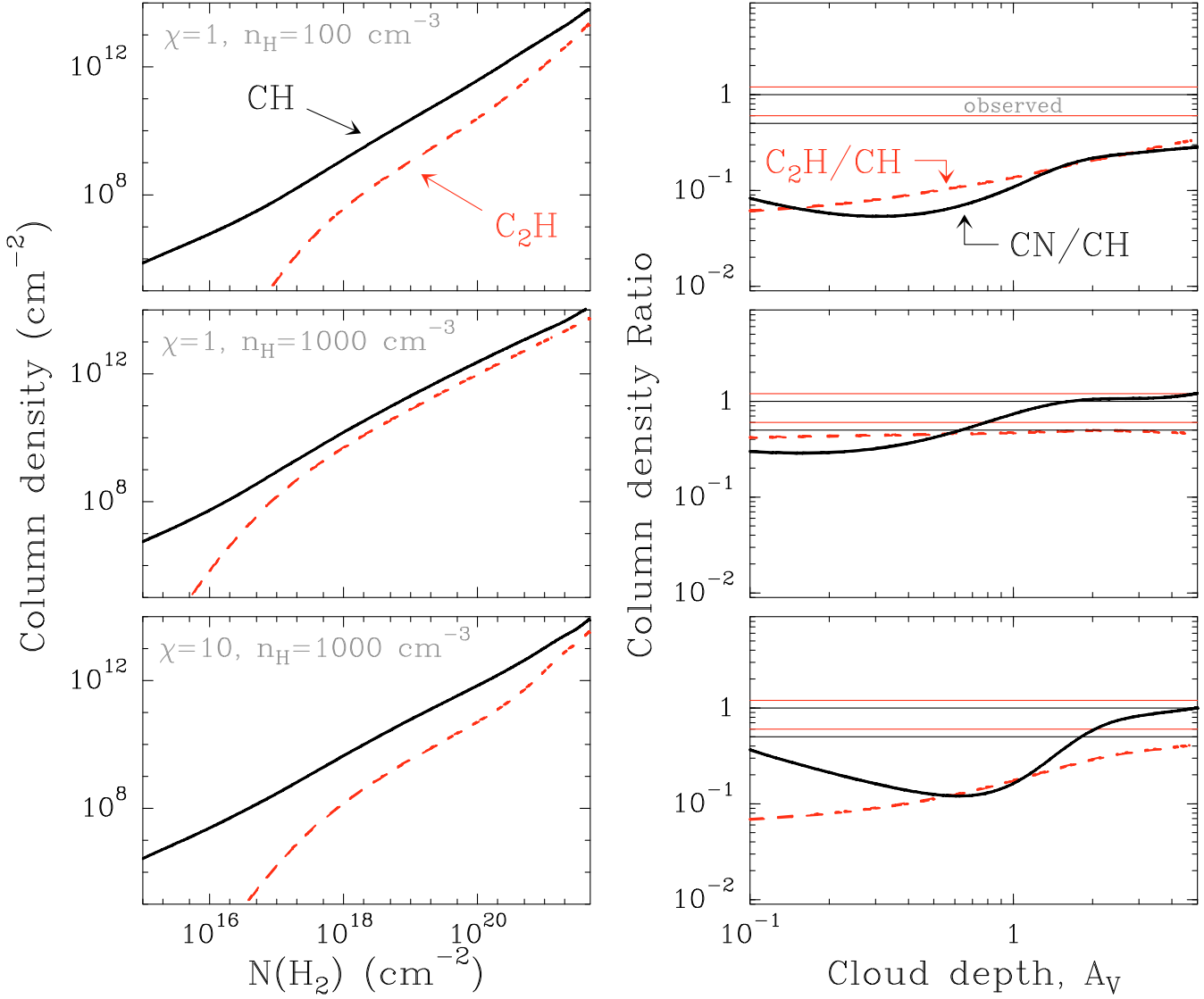


Fig. B.1. *Left:* predicted variation of the CH (black line) and CCH (red dashed line) column density as a function of the H₂ column density for three models, computed with $\zeta_{\text{H}} = 10^{-16} \text{ s}^{-1}$: $\chi = 1$ and $n_{\text{H}} = 100 \text{ cm}^{-3}$ (top), $\chi = 1$ and $n_{\text{H}} = 1000 \text{ cm}^{-3}$ (middle) and $\chi = 10$ and $n_{\text{H}} = 1000 \text{ cm}^{-3}$ (bottom). *Right:* Variation of the CN/CH (black lines) and CCH/CH (red dashed lines) column density ratios for the same models. The gas density n_{H} is defined as $n(\text{H}) + 2n(\text{H}_2)$. The observed ranges are indicated.